

Characteristics of sub-keV atom-Si(111) surface collisions

Magnus Hedström and Hai-Ping Cheng

Quantum Theory Project and Department of Physics, University of Florida, Gainesville, Florida 32611

(Received 18 September 1998)

Molecular-dynamics (MD) simulations, using the potential developed by Tersoff, are reported for Si bombardment of Si(111) in the collisional energy range 15–520 eV. A comparison between ordinary MD and a modified version that includes a model for electronic stopping power and electron-phonon coupling is made. It is found that such modification does not significantly change the results for penetration depth and surface damage. However, electronic stopping does lead to energy dissipation and approximately 10–15% of the collisional energy is transferred to the electrons. The surface damage reaches deeper than the penetration of the projectile and is identified as single atom displacements or small-sized amorphous regions.

[S0163-1829(99)16115-0]

I. INTRODUCTION

Collisions between ions and semiconductors has been a topic of intense experimental and theoretical investigation for several decades. Low-energy ion bombardment of surfaces includes a rich variety of physical phenomena of both fundamental and applied nature. Important examples are, e.g., ion implantation, sputtering, deposition, surface modification, electronic excitation, and phase transitions.

Technologically, ion implantation has become a widely used doping technique for fabrication of very large scale integration (VLSI) devices.¹ The ongoing reduction in size of the VLSI chips, while at the same time the number of components per chip increases, is one driving force for obtaining a more detailed understanding of ion implantation, in order to gain more control over the manufacturing process of VLSI devices.

Experimental techniques mainly probe the final result of the collision process, such as sputtering yields or damage production. At present, the experimental time resolution does not allow for the study of the full dynamics of these processes. Molecular-dynamics (MD) simulations, on the other hand, do permit a detailed study at the atomic level of such processes. MD studies of ion-semiconductor bombardment were reported already in the 1970's. One of the first of these papers is the study of Ar⁺ collisions with germanium by Ostry and MacDonald.²

MD simulations of sub-keV bombardment of silicon have been carried out by Kitabatake and co-workers^{3–5} and recently by Hensel and Urbassek,⁶ who examine the Si self-bombardment of the (100), (110), and (111) surfaces at energies up to 100 eV. Investigations of collisions in the keV regime using MD have been done by Diaz de la Rubia and co-workers.^{7,8} One of the objectives for their studies is to analyze the damage production in terms of structural transformations and formation of amorphous pockets in silicon. In a recent paper a comparative study of semiconductors and a number of fcc metals is presented.⁹ Sputtering yields from ion collisions with silicon have been calculated from MD simulations by Stansfield, Broomfield, and Clary¹⁰ and Smith, Harrison, and Garrison.¹¹

Damage production in the keV regime and above may

also be studied using methods based on the binary collision approximation.¹² However, in order to obtain detailed information regarding the dynamics, MD simulations are necessary.¹³

In this paper we present results from MD studies of Si collisions with Si(111) surface, with collisional energy in the range from 15 to 500 eV. This energy range has not been systematically covered in previous calculations. Thus our calculations bridge the gap between investigations in the sub-100-eV range^{3–6} and the keV regime.^{7–9} The target for our study is to understand how collisional energy influences penetration depth and defect production in terms of collision mechanisms. We also implement a model for electronic stopping power and electron-phonon interactions,¹⁴ into the MD code that had previously been used for predictions concerning soft landing and glass formation in nanocrystals^{15,16} and recently for cluster surface collisions.¹⁷ The simulations that include electronic stopping are compared to ordinary MD calculations in order to understand when, and for what properties, inclusion of electronic stopping is needed.

In the next section we give details concerning the system and describe the simulation method. Results are presented in Sec. III, followed by discussion and conclusions in Sec. IV.

II. SYSTEM AND SIMULATION METHOD

The Si(111) surface is taken to be a slab consisting of 33 double layers, each containing 288 atoms, so the total size of the substrate is 9504 atoms. The slab is 103 Å deep with a rhombic surface of dimensions 46×46 Å. A few layers at the bottom are held fixed in order to stabilize the system. All the other atoms are dynamical, i.e., they are allowed to move according to the forces exerted by their neighbors. Temperature control is applied only to the deepest layer of dynamical atoms, i.e., these atoms are coupled to a heat bath held at a fixed temperature, $T_0 = 150$ K, to maintain constant temperature. The temperature control at the bottom also has the function to absorb eventual shock waves that may reach the deepest layers of atoms. Initially the surface atoms occupy the sites of a perfect diamond lattice with conventional lattice constant 5.43 Å. Before any collision event, the surface is thermalized, to simulate the specific temperature T_0 . This is

achieved by giving all the dynamical atoms velocities commensurate with the Maxwell-Boltzmann distribution for the given temperature.

Taking the z axis to be normal to the surface, periodic boundary conditions are applied to all the surface atoms in the x and y directions, but not along the z axis. The projectile is released at a distance of 10 Bohr above the surface, where its interaction with the surface is zero, and is given a momentum towards the surface at normal incidence.

The Tersoff potential¹⁸ is used to calculate the forces between silicon atoms. This potential was chosen since it does not only fit to the diamond structure, but also to structures with a coordination number different from four. In particular, compared to the Stillinger-Weber potential,¹⁹ the Tersoff potential gives a better description of amorphous silicon. The potential by Stillinger and Weber is more commonly used in studies on radiation damage in Si, although it is known to favor the tetrahedral bonding too strongly. Recently in a study by Nordlund *et al.*⁹ a systematic comparison between the two interatomic potentials was made and indeed, the number of defects produced due to ion impact of the Si surface was twice as many when using the Tersoff potential as compared to the results from using the Stillinger-Weber potential. This manifests the fact that the Tersoff potential do not discriminate overcoordinated and undercoordinated structures, as does the Stillinger-Weber potential.

The motion of all the dynamical surface atoms and the projectile is governed by Newton's equations,

$$m_i \ddot{\mathbf{x}}_i = -\nabla_i U(\mathbf{x}_1, \mathbf{x}_2, \dots, \mathbf{x}_N), \quad (1)$$

where \mathbf{x}_i are coordinates of the i th atom and U is the potential, which are solved using Gear's fifth-order predictor-corrector method.²⁰

For a set of silicon self-collisions inelastic energy losses were also included. Specifically electronic stopping and also electron-phonon coupling were modeled using a frictional force $-\beta \dot{\mathbf{x}}$ and a random force, $\eta(t)$ so the equation of motion takes the Langevin form¹⁴

$$m_i \ddot{\mathbf{x}}_i = -\nabla_i U(\mathbf{x}_1, \mathbf{x}_2, \dots, \mathbf{x}_N) - \beta \dot{\mathbf{x}}_i + \eta(t). \quad (2)$$

In these simulations all atoms with kinetic energy higher than $10 \times \frac{3}{2} k_B T_0$ were subjected to the frictional and the random forces. The value of β was chosen as 5.8×10^{-11} g/s, which is in between the value calculated from the electronic stopping power theory of Lindhard and Scharff²¹ and recent experimental measurement.²² In previous work^{8,9} friction has not been applied as generously as here, but applied only to atoms with kinetic energy higher 1 eV. Our results thus emphasize the effect of electronic stopping more than the work cited above.

III. RESULTS

A. Comparison between Newtonian and Langevin MD

1. Penetration depth

In order to study the effect of Si bombardment of Si(111) surface we select five different initial impact points from the irreducible symmetry zone at normal incidence as shown in Fig. 1. The simulations are performed at four different initial velocities, $v_0 = 10, 20, 40,$ and 60 km/s, for the incoming Si

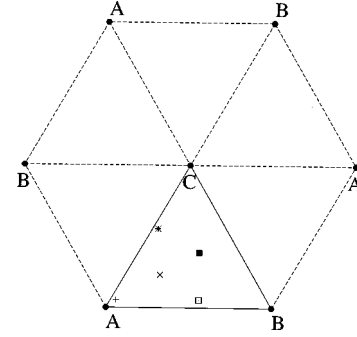


FIG. 1. Part of the Si(111) surface with the impact points shown in the irreducible symmetry zone at normal incidence. A, B, and C indicate the stacking of the (111) double layers.

atom, corresponding to a collisional energy range between 15 and 520 eV. For one of the initial impact points a comparison between Eq. (1) and Eq. (2) is done. In Fig. 2, the penetration depth of the incoming Si into the substrate is shown for various velocities and for both Newtonian and Langevin MD (NMD and LMD, respectively). Here we have selected the largest penetration depth for the incoming particle, although in most cases it finally ends up at a slightly shallower depth after long simulation time. It is clear that, for the projectile velocities considered here, electronic stopping does not influence the penetration depth, and later a deeper analysis of the particle trajectories will confirm that the stopping comes only from a very few atomic collisional events. For $v_0 = 80$ km/s we notice a large difference in penetration depth for this particular impact point. The difference can however not be attributed to electronic stopping but the two trajectories explore different parts of phase space and in this case it gives rise to a large difference. The stopping is still due to atomic recoils. A different initial impact point may give a reverse situation where the atom that experiences electronic stopping may penetrate deeper than the atom in the other simulation. A careful analysis of the result for 40 km/s shows that that is actually the case. One may conclude that for calculating penetration depth, it is safe to not include frictional forces.

2. Number of defects

Another interesting quantity to compare with is the damage the projectile causes to the surface. A measure of this is

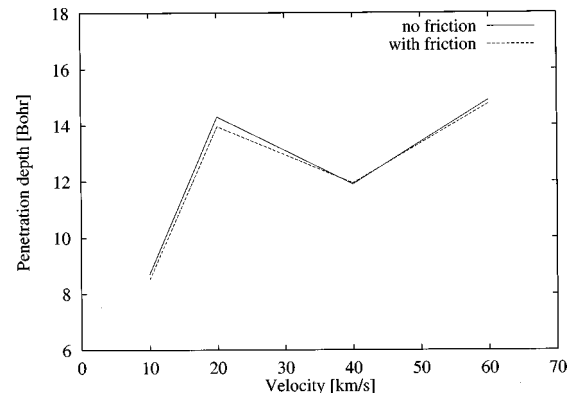


FIG. 2. Penetration depth of the incoming Si into the surface as a function of initial velocity. A comparison between Newtonian and Langevin MD for a particular impact point.

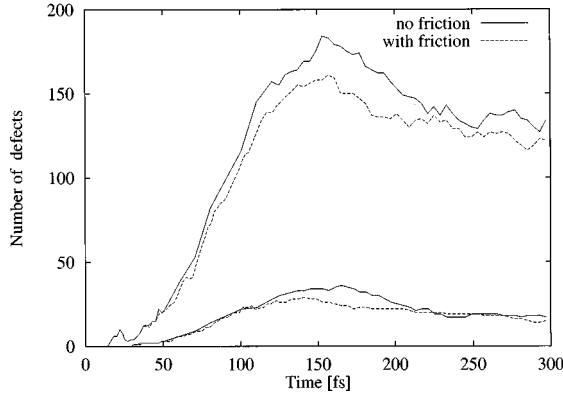


FIG. 3. The number of defects due to projectile impact as a function of time. The upper curves show the number of high-energy particles and the lower curves the number of displaced particles. A comparison between ordinary MD and simulations including electronic stopping (friction) at an initial velocity 40 km/s.

to calculate the number of disordered atoms. Different conventions for doing this may be chosen. One way is to calculate the number of atoms that have been excited more than 0.25 eV, $N_{\text{high } E}$. Another way to estimate the damage caused to the surface is to calculate the number of displaced atoms, N_{displ} . Various methods to calculate this quantity have been proposed in the literature^{8,9} and here we let N_{displ} be the number of atoms that have been displaced more than half the Si-Si equilibrium bond distance, $r_{\text{NN}} = 2.35 \text{ \AA}$, from their original lattice points. In Fig. 3 the number of defects as a function of time is shown for both NMD and LMD. These results are obtained for an initial projectile velocity of 40 km/s, which happen to give almost identical particle trajectories for both NMD and LMD. This initial condition is therefore suitable for comparison of also other quantities than penetration depth.

The upper two curves in Fig. 3 show the number of atoms with total energy higher than -0.16 Hartree (~ 0.25 eV above the average atom energy at $T_0 = 150$ K) and the lower two curves show the number of atoms displaced more than $r_{\text{NN}}/2$ from their original lattice sites. After 220 fs the number of displaced particles have reached approximately the same value and the two curves continue to be very close at subsequent times. The main difference between the two cases is that the peak value at 170 fs is significantly lower for LMD compared to NMD. However, after long propagation time, electronic stopping seems not to influence the number of defects produced. This is even more true for the lower velocities, but also in the case of 60 km/s initial velocity of the projectile. This is also in agreement with previous observations.⁸ The picture is somewhat different when it comes to $N_{\text{high } E}$. In LMD, the number of excited atoms are at all times lower compared to the results obtained from NMD. For the lower velocities the results differ less between NMD and LMD. With either measure of defects, displaced particles or excited particles, LMD gives smaller peak values. As was mentioned in the previous section, electronic stopping is applied to a larger extent here than in previous work. Even so, for velocities up to 60 km/s the effect is so small that the electronic stopping may be omitted. However, electronic friction may be an important factor for dissipating energy in the collision cascade.

TABLE I. Energy loss ΔE due to electronic stopping, at initial velocities v_0 . $\Delta E(\text{MD})$ is obtained from MD simulations and $\Delta E(\text{THY})$ is calculated from Eq. (3). Details are further explained in the text.

v_0 km/s	$\Delta E(\text{MD})$ eV	$\Delta E(\text{THY})$ eV	$\Delta E_{i+1}/\Delta E_i$
10	1.5	7.8	4.9 (4.0)
20	7.4	31.2	4.3 (4.0)
40	31.8	125	2.4 (2.25)
60	76.2	281	

3. Energy loss

In order to verify whether electronic stopping power is important for energy dissipation at these energies or not, we monitor the energy loss due to the term $-\beta \dot{\mathbf{x}}$ in Eq. (2), during the time evolution. The results at $t = 300$ fs are reported in Table I [$\Delta E(\text{MD})$]. For comparison we also give the theoretical energy loss $\Delta E(\text{THY})$, that would be obtained in the case of $U = 0$ in Eq. (2), i.e., the stopping arises only from electronic friction. Under such assumption one may integrate Eq. (2) for the projectile to obtain

$$\Delta E(\text{THY}) = \frac{mv_0^2}{2} \left[1 - \exp\left(\frac{-2\beta}{m} t\right) \right]. \quad (3)$$

The ratio $\Delta E_i/\Delta E_j$ between the energy losses obtained from two different initial velocities $v_{0,i}$ and $v_{0,j}$ is given by $v_{0,i}^2/v_{0,j}^2$, assuming Eq. (3) is valid. The actual values $\Delta E_{i+1}/\Delta E_i$ from LMD simulations are given in the last column of Table I, with the ideal ($v_{0,i}^2/v_{0,j}^2$) values within parenthesis. It is worth to note that these values are very similar and that the agreement between the values from LMD and the simple electronic stopping considerations becomes closer as the velocity increases.

Even more important to note is that $\Delta E(\text{THY})$ is between 3.7 and 5.2 times larger than $\Delta E(\text{MD})$. This indicates that even when kinetic energy is allowed to dissipate into the electronic system, most of the collisional energy is transferred to the lattice, for the velocities considered here.

The fact that the MD simulations at higher impact velocities give comparatively higher energy loss to the electrons, may be understood as follows: A projectile with high velocity generates more atoms in the collision cascade, with kinetic energy above the barrier value $10 \times 3/2k_B T_0$, at which they will be subjected to Eq. (2). A higher barrier height, e.g., 1 eV, will result in less energy loss to the electrons. Thus the results presented here give an upper limit for the energy loss.

B. Statistics from conventional MD

1. Depth distribution

Five different impact points have been used in order to obtain more statistics in the case of Si self-bombardment using Eq. (1). The average penetration depth of the projectile

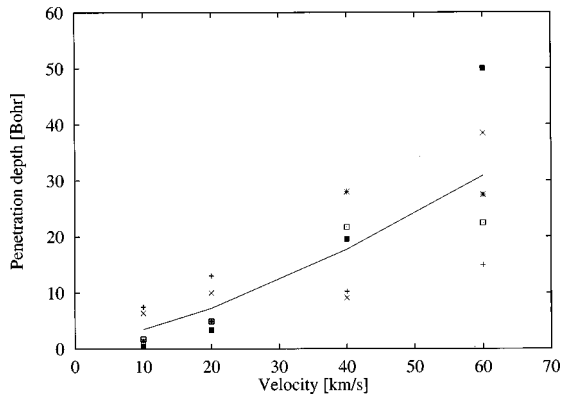


FIG. 4. Penetration depth as a function of initial velocity. The solid line represents the average of five different events, also marked in the diagram, with different symbols for the different impact points.

is almost proportional to its initial velocity as can be seen from the solid line in Fig. 4. Also indicated in the figure are the penetration depths for each individual impact point. Clearly for each individual impact point the relation between penetration depth and initial velocity is much more complicated and may even not be an increasing function. For the events marked with crosses we see that the penetration depth at 20 km/s is deeper than for 40 km/s and, e.g., the impact point represented by open squares favors 40 km/s over 60 km/s. We also notice in Fig. 4 that the range in penetration depth increases with increasing velocity, from 7 Bohr at 10 km/s to 35 Bohr at 60 km/s. However, the statistics from only five events do not permit a meaningful calculation of the variance of the depth distribution.

2. Collision mechanisms

As was mentioned earlier, only a few atomic collision events are majorly responsible for the stopping of the projectile. To illustrate this, one of the trajectories at $v_0 = 60$ km/s is shown in Fig. 5. The solid line shows the projectile trajectory

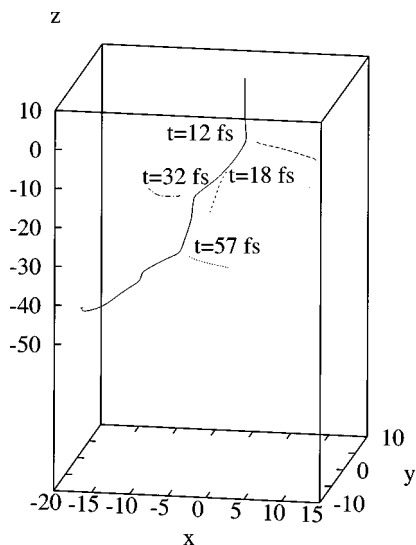


FIG. 5. Real-space trajectory for a $v_0 = 60$ km/s projectile (solid line) and some of the atoms that gain high momentum after collision (dashed lines).

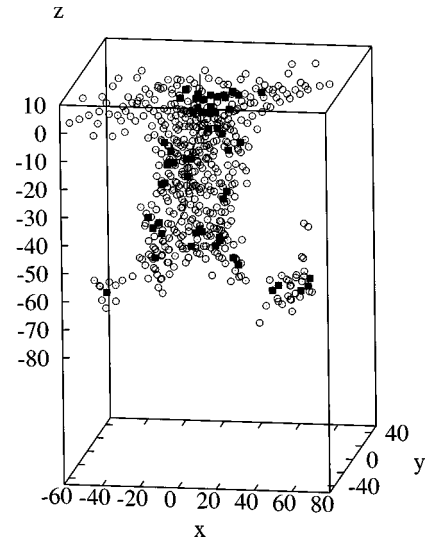


FIG. 6. Surface damage at $t = 300$ fs due to the collision cascade caused by the particle in Fig. 5. Open circles depict high energy particles and solid squares show displaced particles.

tory and dashed lines show the trajectories of those atoms that receive the highest impacts. In the collision at $t = 12$ fs the projectile loses about 100 eV and at $t = 32$ fs only 270 eV of its initial 520 eV of kinetic energy remain. Between $t = 32$ and $t = 57$ fs occurs what could be characterized as channeling. The projectile travels more than 20 Bohr without significant loss in velocity.

The surface damage at $t = 300$ fs, caused by the collision cascade is shown in Fig. 6. The initial conditions are the same as in previous figure. The surface damage is mainly centered around the trajectory of the projectile but reaches deeper (70 Bohr) than the projectile (50 Bohr). Open circles show high-energy atoms and these are more clustered together around the projectile trajectory than the displaced atoms (solid squares), which are more sparsely scattered and seem to occur either as single particle defects or in very small clusters, amorphous regions.

The sequence of Figs. 7(a)–7(d) shows the distribution of “hot” atoms in the surface at different times for the collision cascade in Figs. 5 and 6. In analogy with the equipartition principle we identify the temperature of an atom through its kinetic energy via the relation $m_i v^2 / 2 = 3/2 \times k_B T$. In Figs. 7(a)–7(d) open circles represent atoms with temperatures between $5T_0$ and $10T_0$, i.e., 750–1500 K, and solid circles shows atoms with temperatures above $10T_0$. At $t = 50$ fs, Fig. 7(a), there are a few hot atoms in the immediate vicinity of the trajectory of the projectile. The ratio of solid to open circles is 18:6. At $t = 100$ fs, Fig. 7(b), this ratio is 70:54. The hot atoms clearly occupy a larger region of the slab and one may also notice that the open circles are far more abundant in the upper layers of the surface that were covered by the projectile in the first 50 fs [Fig. 7(a)]. This suggests that most of the particles with $5T_0 < T < 10T_0$ are formed in the collision cascade of secondary particles. Between 50 and 100 fs the number of atoms with $10T_0 < T$ increased considerably and in the next 50 fs [Fig. 7(c)] this number decreases slightly. However, the number of atoms with $5T_0 < T < 10T_0$ continues to increase and the ratio at $t = 150$ fs is 67:71. At $t = 300$ fs [Fig. 7(d)] the number of atoms with

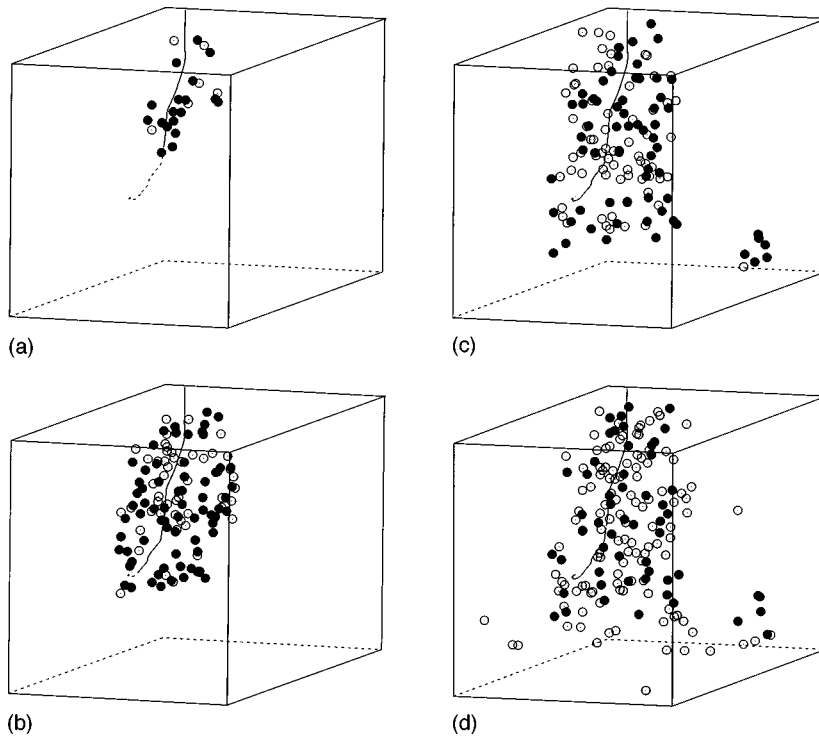


FIG. 7. Snapshots of the location of hot particles at different times, (a) 50, (b) 100, (c) 150, and (d) 300 fs. Open circles shows particles with kinetic temperature between $5T_0$ and $10T_0$ and filled circles shows particles with kinetic temperature larger than $10T_0$. The solid line shows the path that the projectile has covered at the specific time and the dashed line shows the remaining part of its trajectory.

$10T_0 < T$ has decreased to 55, and the number of atoms with $5T_0 < T < 10T_0$ has increased to 117. In the sequence of figures, the region of hot atoms is expanding out from the trajectory of the projectile. This shows how the heat is transferred to the surrounding lattice. Note that the hot atoms near the right boundary of the slab in Figs. 7(c) and 7(d) have

been translated from the left due to the periodic boundary conditions.

The number of defects as a function of time is shown for $v_0 = 20, 40,$ and 60 km/s in Fig. 8. As before the upper curves display $N_{\text{high } E}$ and the lower ones N_{displ} . According to Nordlund *et al.*⁹ the number of defects, when using the

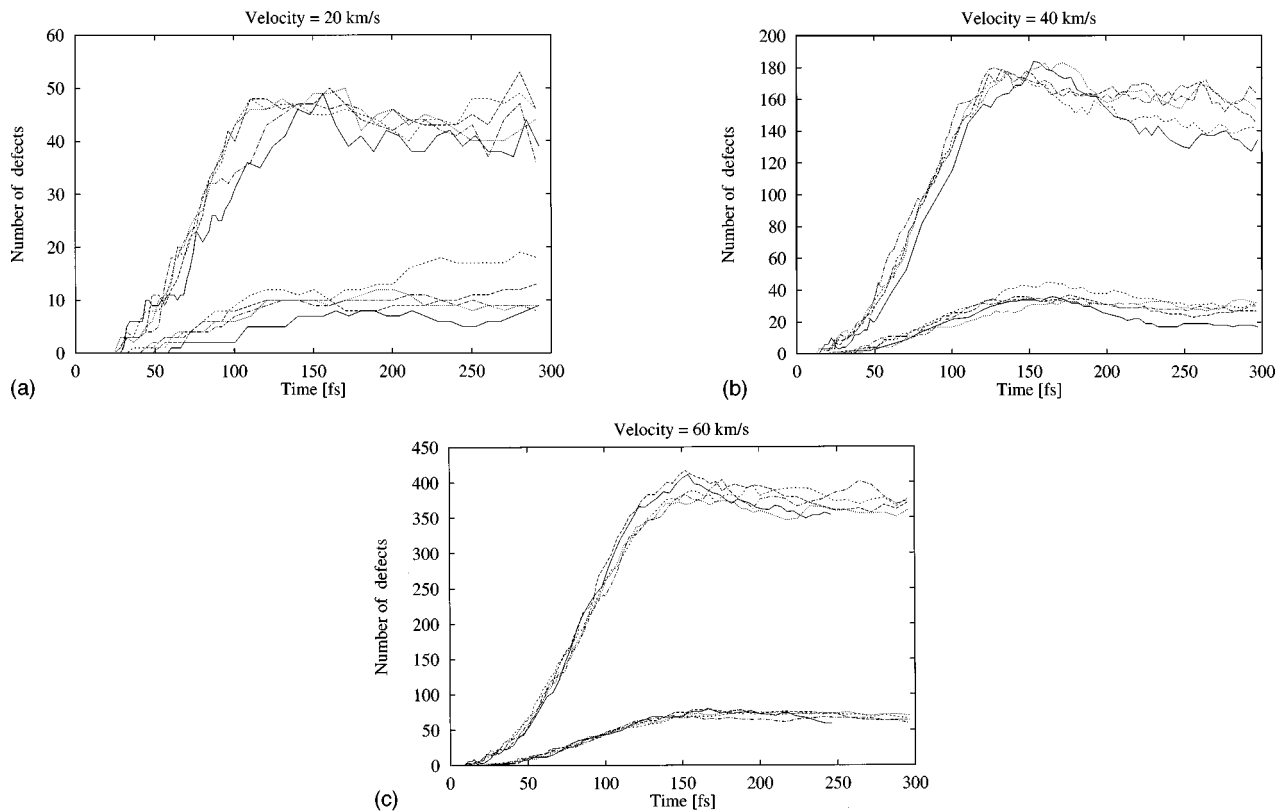


FIG. 8. The number of defects due to projectile impact as a function of time, and initial velocities (a) $v_0 = 20$, (b) $v_0 = 40$, and (c) $v_0 = 60$ km/s. The upper curves show the number of high-energy particles and the lower curves the number of displaced particles.

TABLE II. Average values of the number of high-energy atoms $\bar{N}_{\text{high } E}$, the number of displaced atoms \bar{N}_{displ} , and the penetration depth \bar{Z}_D , for different initial velocities v_0 . The averages are calculated from five different events.

v_0 km/s	\bar{N}_{displ}	$\bar{N}_{\text{high } E}$	\bar{Z}_D Bohr
10	4.2	13.4	3.5
20	11.4	42.2	7.3
40	27.4	147.8	17.7
60	63.8	368	30.9

Tersoff potential, is stabilized at about 1000 fs in the case of 2 keV collision energy. In the simulations presented here the highest energy is only 0.5 keV and we assume that 300 fs should be a sufficient propagation time to reach a stable number of defects. An inspection of Fig. 8 shows that our assumption is valid. The average of $N_{\text{high } E}$, N_{displ} and of the penetration depth Z_D are summarized in Table II.

IV. DISCUSSION AND CONCLUSION

Inclusion of electronic stopping power and electron-phonon coupling in MD simulations of Si bombardment of Si(111) surface, do not influence properties such as penetration depth or defect production. For the collisional energies 15–520 eV used in the study reported here, atomic recoil is by far the dominating mechanism for stopping of the incoming projectile. This also explains why the number of defects

produced in the surface, during the collision cascade, is almost the same in simulations with or without electronic stopping included. This conclusion is valid for all initial impact velocities (10, 20, 40, and 60 km/s) considered in this study and we have indications that this is the case also when the initial velocity is as high as 80 km/s, which corresponds to a collision energy of 930 eV.

However, electronic friction does contribute somewhat to energy dissipation. The simulations show that the energy loss due to electronic stopping power is 10–15% of the total collisional energy. The higher figure refers to the simulation with the highest projectile velocity and the lower number to the lowest velocity. These numbers may be considered as upper bounds since electronic friction is included more generously in our calculations compared to what have been reported previously.

After establishing that friction only has a marginal effect on the dynamics we continue to obtain more statistics from ordinary MD simulations, excluding electronic stopping. These calculations indicate that the average penetration depth as well as the range in penetration depth increases almost linearly with velocity.

ACKNOWLEDGMENTS

The authors acknowledge valuable discussions with Dr. Richard Mathar. The computer simulations were performed using the facilities at the Quantum Theory Project, University of Florida and at the NIST computing center. Financial support was provided by the Department of Energy under Contract No. DE-FG02-97ER45660.

- ¹*Handbook of Ion Implantation*, edited by J. F. Ziegler (North-Holland, Amsterdam, 1992).
- ²D. Ostry and R. J. MacDonald, *Phys. Lett. A* **32**, 303 (1970).
- ³M. Kitabatake, P. Fons, and J. E. Greene, *J. Vac. Sci. Technol. A* **8**, 3726 (1990).
- ⁴M. Kitabatake, P. Fons, and J. E. Greene, *J. Vac. Sci. Technol. A* **9**, 91 (1991).
- ⁵M. Kitabatake and J. E. Greene, *Thin Solid Films* **272**, 271 (1996).
- ⁶H. Hensel and H. M. Urbassek, *Phys. Rev. B* **57**, 4756 (1998).
- ⁷T. Diaz de la Rubia and G. H. Gilmer, *Phys. Rev. Lett.* **74**, 2507 (1995).
- ⁸M.-J. Caturla, T. Diaz de la Rubia, L. A. Marqués, and G. H. Gilmer, *Phys. Rev. B* **54**, 16 683 (1996).
- ⁹K. Nordlund, M. Ghaly, R. S. Averback, M. Caturla, T. Diaz de la Rubia, and T. Tarus, *Phys. Rev. B* **57**, 7556 (1998).
- ¹⁰R. A. Stansfield, K. Broomfield, and D. C. Clary, *Phys. Rev. B* **39**, 7680 (1989).

- ¹¹R. Smith, D. E. Harrison, and B. J. Garrison, *Phys. Rev. B* **40**, 93 (1989).
- ¹²P. Sigmund, *Rev. Roum. Phys.* **17**, 823 (1972).
- ¹³R. Smith, *Atomic and Ion Collisions in Solids and at Surfaces* (Cambridge University Press, Cambridge, 1997).
- ¹⁴A. Caro and M. Victoria, *Phys. Rev. A* **40**, 2287 (1989).
- ¹⁵H.-P. Cheng and U. Landman, *J. Phys. Chem.* **98**, 3527 (1994).
- ¹⁶H.-P. Cheng and U. Landman, *Science* **260**, 1304 (1993).
- ¹⁷H.-P. Cheng, *Phys. Rev. B* (to be published day Month 19xx).
- ¹⁸J. Tersoff, *Phys. Rev. B* **39**, 5566 (1989).
- ¹⁹F. H. Stillinger and T. A. Weber, *Phys. Rev. B* **31**, 5262 (1985).
- ²⁰M. P. Allen and D. J. Tildesley, *Computer Simulations of Liquids* (Clarendon, Oxford, 1987).
- ²¹J. Lindhard and M. Scharff, *Phys. Rev.* **124**, 128 (1961).
- ²²K. A. J. Keinonen and P. Tikkanen, *Appl. Phys. Lett.* **60**, 228 (1992).